Tomographic DST algorithm for stone column site imaging and characterization

Erick Baziw
Baziw Consulting Engineers Ltd., Vancouver, Canada
Gerald Verbeek
Baziw Consulting Engineers Ltd., Vancouver, Canada

ABSTRACT:

Stone columns are used in geotechnical site remediation to increase load-bearing capacity and reduce settlement of foundations. Stone columns also improve slope stability and increase the shear strength of a soil. A very challenging problem is to characterize the in-situ shear wave velocities from data acquired from Downhole Seismic Testing (DST) after the insertion of stone columns. DST is an important geotechnical testing tool for site characterization that provides low strain ($<10^{-5}$) in-situ interval compression and shear wave velocity estimates. The seismic data acquired from DST in the presence of stone columns is very challenging due to the resulting complicated *in-situ* soil conditions. The DST post analysis requires that a mandatory and proper tomography algorithm is implemented that incorporates source wave raypath refraction. Baziw Consulting Engineers has invested considerable resources in developing DST imaging algorithms such as the Normal Moveout Seismic Cone Tomographic Testing (NMO-SCTT) algorithm. This paper outlines significant modifications/additions made to the NMO-SCTT algorithm to facilitate stone column site characterization. The unique nature of the stone column site conditions allows for important *a priori* conditions to be specified which dramatically reduces the optimal solution space for the estimated interval velocities.

1. INTRODUCTION

Stone columns are used to increase load-bearing capacity, reduce settlement of foundations, improve slope stability, and increase the shear strength of a soil which prevents liquefaction. Stone columns also accelerate soil consolidation due to the drainage capacity of the granular materials within the columns. The four major types of stone column construction are vibro-replacement, vibro-displacement, compacted stone columns, and vibro-compaction. There is extensive technical and commercial literature available which describes these four construction techniques and the associate ground improvement benefits (Billoet and Gauthey, 2011; Carvajal et al., 2013; Fernando et al., 2015; Kirsch, 2006; Selcuk and Kayabali, 2015; Mccabe and Mcneill, 2006; Ng and Tan, 2015; Sexton et al., 2016; Sondermann et al., 2016).

In general terms, in stone column construction a vibrating tool suspended from a crane penetrates to the design depth by means of vibration and of its own weight. Crushed stone is then inserted into the hole. The vibrating probe densifies the soil by breaking down the pores of the surrounding soil. The stone that is inserted into the hole takes the place of the soil and retains pressure on the soil that was created by the vibrating probe. The stone consists of crushed coarse aggregates of various sizes. Figure 1 illustrates a schematic diagram (Sondermann et al., 2016; Mccabe and Mcneill, 2006) showing a typical installation process by vibro-displacement where the dry-top and bottom-feed method is implemented. In this case stone column construction is carried out using compressed air and no water flush. Referring to Fig. 1, the vibro-displacement process is four-fold. 1) The vibrocat is stabilized on hydraulic outriggers where the leaders are elevated to the vertical and the vibrator is located on the ground at the stone column position. The skip is charged with stone. 2. The skip travels up the leaders and automatically loads stone into the reception chamber at the top of the vibrator. 3. The vibrator penetrates to design depth using its own weight, a ‘pull down’ force, compressed air and vibrations. 4. At the required depth, stone is released and compacted by small upward and downward movements of the vibrator. The up-down motion and centrifugal force of the depth vibrator allows formation of a compacted, granular column as well as densification the surrounding soil in between the columns.

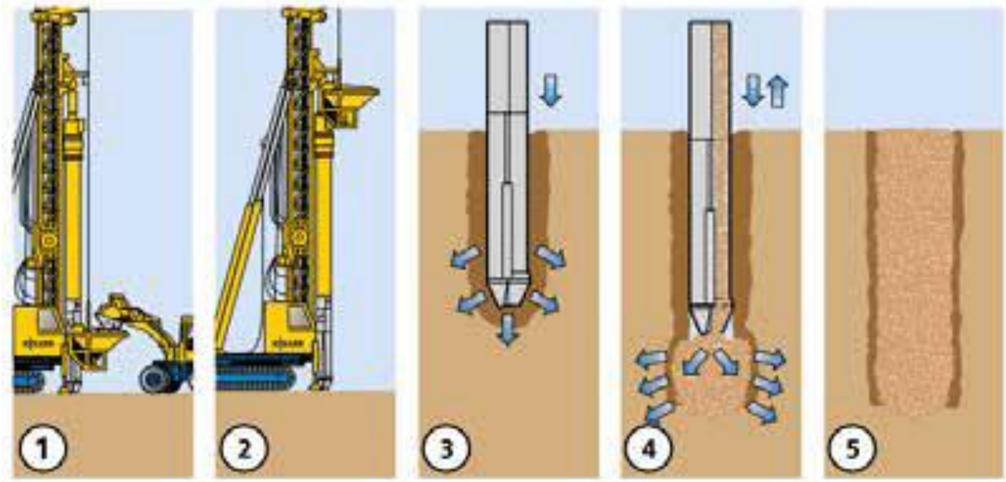

Figure 1: Schematic diagram showing typical installation process of stone columns by vibro-displacement where the dry-top and bottom-feed method is implemented (Sondermann et al., 2016; Mccabe and Mcneill, 2006).

Stone columns are inserted throughout the area in either triangular, square, or hexagonal grid pattern as illustrated in Fig. 2. The most common grid pattern are triangular or rectangular. The stone column depth depends on the in-situ soil properties. Typical column diameters range from 0.6 m to 1.1 m (Billoet and Gauthey, 2011; Sondermann et al., 2016) and typical center-to-center spacings range from 1.5 m to 2.5 m.

A very challenging problem is to characterize the in-situ shear wave velocities after the insertion of stone columns. This is due to the resulting very complicated in-situ soil conditions and the correct interpretation of source wave arrivals time. Furthermore, it is mandatory that a proper tomography algorithm is implemented along with raypath refraction. This paper outlines DST tomographic stone column

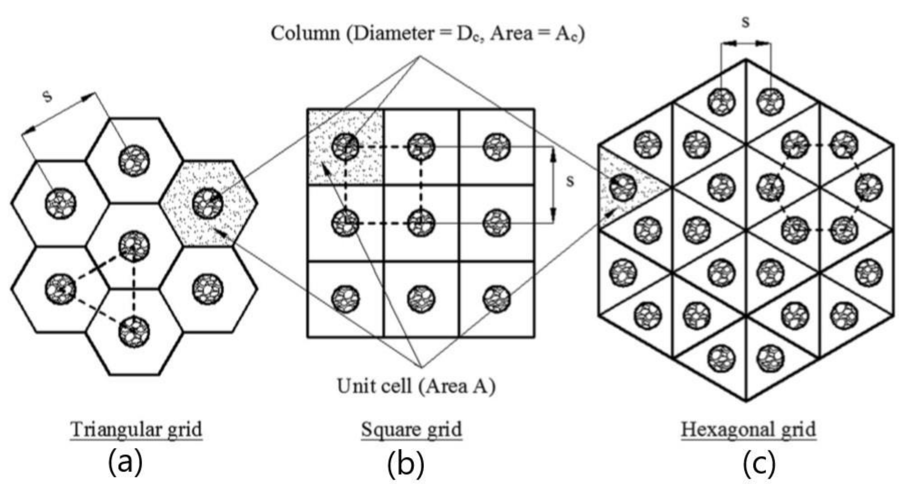

Figure 2: Typical column grids encountered in practice. (a) Triangular; (b) Square; (c) Hexagonal (after Sexton et al., 2016).

imaging algorithm where the unique nature of the stone column site conditions allow for important *a priori* conditions to be specified. This dramatically reduces the optimal solution space for the estimated interval velocities. This new technique is referred to as the Forward Modeling Downhill Simplex Method - Stone Columns (FMDSMSC).

2. DST STONE COLUMN SITE CHARACTERIZATION

Downhole Seismic Testing (DST) has proven to be a very effective tool for the estimation of *in-situ* shear and compression wave velocities low the strain shear modulus (ASTM, 2017; Baziw, 2002; Baziw and Verbeek, 2012 and 2014a and 2014b). Accuracy in the estimation of shear and compression waves velocities is of paramount importance, because these values are squared during the calculation of various geotechnical parameters such as the shear modulus, Poisson's ratio and Young's modulus. Figure 3 shows a schematic of the typical DST configuration: a seismic source is used to generate a seismic wave train at the ground surface. One or more downhole seismic receivers are used to record the seismic wave train at predefined depth increments. When triggered by the seismic source a data recording system records the response of the downhole receiver(s). Interval velocity estimates are obtained by measuring the relative travel times between the source waves recorded at subsequently greater depths. It has been demonstrated that ray path refraction should be taken into account by implementing iterative forward modeling or data inversion techniques (Baziw, 2002; Baziw and Verbeek, 2012) when estimating interval velocities. Baziw and Verbeek (2018) outlined a new methodology which facilitated the tomographic imaging of the subsurface from DST data sets where normal moveout of the seismic source is implemented.

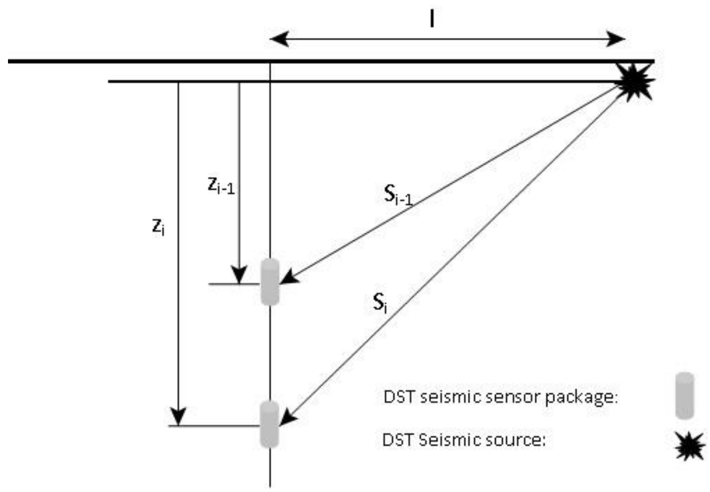

Figure 3: Schematic of the typical DST configuration (Baziw and Verbeek, 2014b).

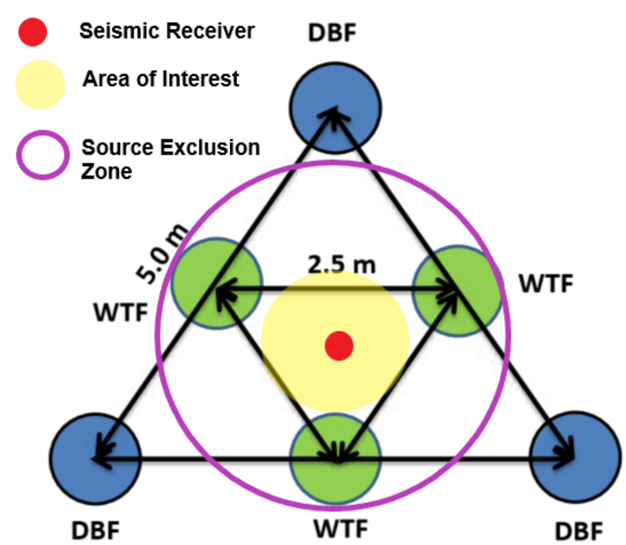

Figure 4: Plane view of arrangement of Stone Column Installation (after, Fernando et al., 2015).

In stone column sites the estimation of in-situ shear waves from DST can be significantly challenging due to the complex nature of closely positioned stoned columns and the desire to minimize complex source waves, near-field source waves and source wave reflections. This is illustrated in Fig. 4 (after, Fernando et al., 2015). In Fig. 4 the stone columns are arranged in an equilateral triangular pattern with a center to center spacing of 2.5m. Stone columns at 5 m centers were installed using the "dry bottom feed (DBF)" method and the columns at 2.5 m spacing were installed using the Wet Top Feed (WTF) method. The stone columns will have an estimated diameter of 0.9 m.

In Fig. 4, the DST Stone Column Site Characterization (DST-SCSC) area to have interval velocities estimated is identified by the light yellow circle, the red circle denotes the DST seismic receiver and the purple circle (approximate 2m radius) identifies the source exclusion zone where the seismic source should be ideally generated outside this area. The seismic source exclusion zone is implemented so that there is minimization of source wave "rod noise" in SCPT (Baziw and Verbeek, 2014b) and minimization of near field waves. The near-field and far-field terms describe the displacement radiation patterns of a typical three-dimensional seismic source. In general terms, the near-field particle motions are complex (they tend not to adhere to Hooke's law) and are ignored in geotechnical engineering. The near-field terms tend to decay as $1/r^2$ where r is the distance from the source while the desirable far-field terms decay due to geometrical spreading (i.e., $1/r$).

Additional constraints on the positioning of the seismic source is that it should not be placed in contact with a stone column. Excitation of the stone column would result in the generation of significantly complex source waves. In addition, it is desired that number of reflected source waves is minimized and that they have significantly longer travel paths then the desired direct source wave. Figure 5 illustrates a seismic hammer beam which generates horizontally polarized shear waves (SH waves). If the SH source is generated at location **A** then the three reflected source waves would have similar travel distances with the desired direct wave resulting in significant source wave interference. This would make the estimation of the direct source wave's arrival time a challenging tasks. If the SH source is generated at location **B** then the two reflected source waves would have signify longer travel paths than the desired direct source wave. This would result in significantly longer time separation of the reflected waves from the desired direct source and minimal source wave interference. This would dramatically simplify the estimation of the direct source wave's arrival time. The major challenge for post analysis of DST data acquired from source position **B** is to model the source waves travelling through the stone column.

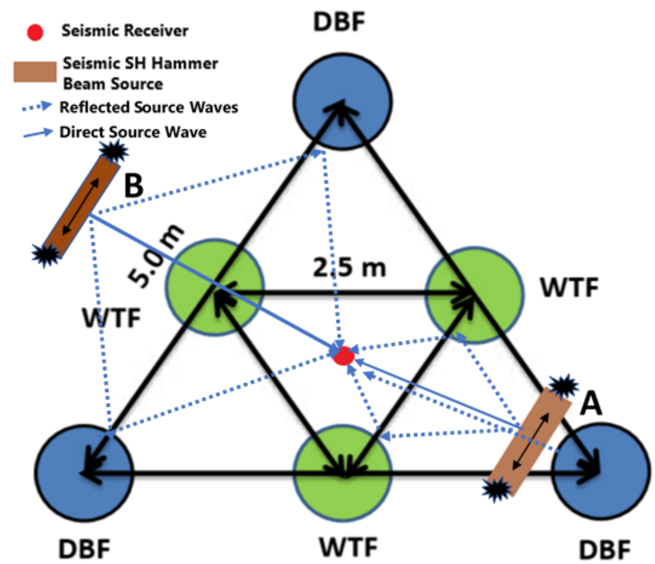

Figure 5: Plane view of possible configurations of DST seismic SH source waves(after, Fernando et al., 2015).

2.1 DST-SCSC Site Configuration

Figure 6 illustrates a cross section schematic of a DST-SCSC where the seismic SH source is located similar to position B outlined in Fig. 5. In Fig. 6, parameter l_1 denotes the radial offset of the DST source from the seismic receiver, l_2 denotes the radius of the stone column, and l_3 denotes the radial offset of the DST source from the stone column. As is shown in Fig. 6, the source waves will travel directly from the source to stone column ***A*** with very small angles of incidence due the relatively high velocity contrast (i.e., $V_2 \gg V_1$ (Baziw and Verbeek, 2014c). The source waves will travel down the stone column refracting into the strengthen medium to be recorded by the seismic probe. The unique site conditions of the stone column ground improvement site allow for important *a priori* conditions to be specified. This significantly reduces the optimal solution space for the interval velocities (V_1 to V_n) to be estimated.

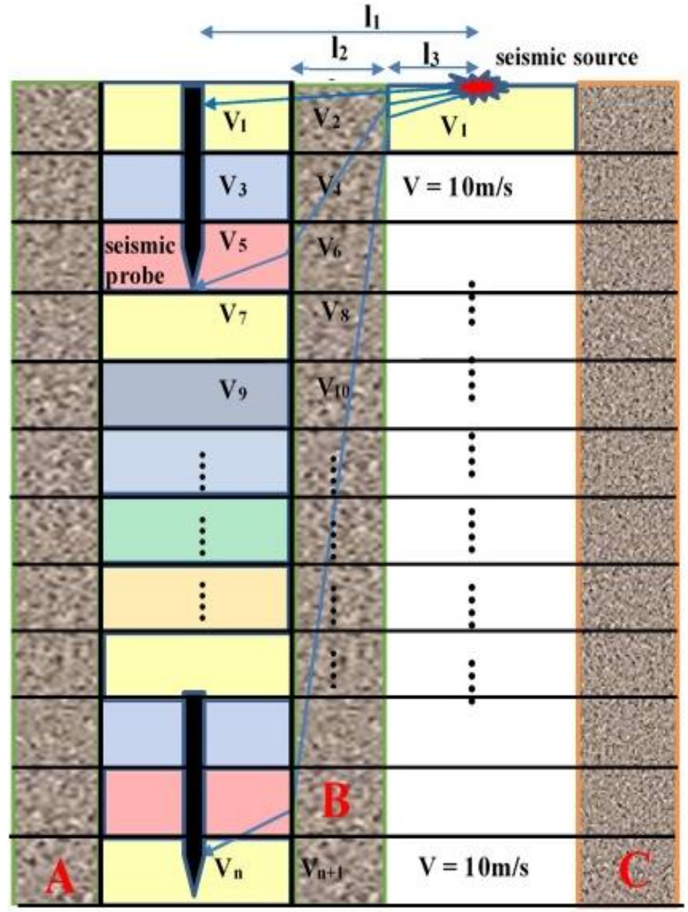

Figure 6: Cross-section of a soil profile where three stone columns have been inserted and source location based upon position B outlined in Fig. 5.

DST-SCSC a priori conditions:

- There is minimal variation in the stone column interval velocities (e.g., $V_2 \approx V_{n+1}$)

- The interval velocities in the densified medium are at least 1.3 times (30%) smaller than those in the stone columns.

$$\left[1.3 \times V_{(2*i-1)} \leq V_{2*i}\right]_{for\ i=1\ to\ n} \qquad (1)$$

- The source waves travel directly from the seismic source to stone column ***A*** with very small angles of incidence. This is due to the relatively high velocity contrast. This condition is implemented in the FMDSMSC algorithm by setting the interval velocities below the first layer V_1 to *V = 10m/s* as illustrated in Fig. 6.

3.0 FMDSMSC TECHNIQUE

The FMDSMSC was developed by implementing the NMO-SCTT algorithm (Baziw and Verbeek, 2018) with significant modifications/additions. The NMO-SCTT algorithm utilizes an iterative technique based on the same mathematical tools (e.g., Newton-Raphson technique and simplex iterative forward modeling) that are used in the single source offset Forward Modeling Downhill Simplex Method (*FMDSM*) technique (Baziw, 2002; Baziw, E. and Verbeek, G, 2012 and 2014) which pioneered the implementation of raypath refraction when estimating source wave interval velocities from DST data sets. Figure 7 illustrates a schematic of the NMO-SCTT testing and analysis configuration. Here the downhole seismic data sets are acquired at various radial source offsets. In the NMO-SCTT, the 2D velocity models are derived for each subsequent offset. For example, the ray path for offset X2 and depth Z2 might travel through areas V2D[1,2], V2D[1,1] and V2D[1,2], in which case for the last two areas the velocity values obtained during the analysis of the data set for offset X1 are used and V2D[1,2] is estimated. This varies from the FMDSMSC where normal moveout of the seismic source is not implemented. In the FMDSMSC case the three *a priori* DST-SCSC constraints are implemented for a constant source radial offset (l_1 in Fig. 6). This is similar to the standard FMDSM where a constant source radial offset is implemented. Comparing Figs. 6 and 7, it is also clear that another significant difference between the NMO-SCTT and FMDSMSC algorithms is that the NMO-SCTT models slant planes while the FMDSMSC models vertical planes. This requires significant changes in the ray tracing portion of the FMDSMSC algorithm as subsequently outlined.

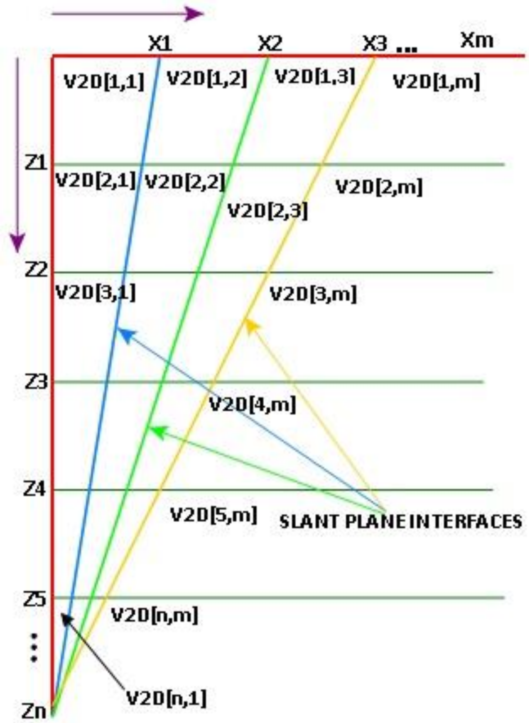

Figure 7: Schematic of a NMO-SCTT testing and analysis configuration (Baziw and Verbeek, 2018).

3.1 FMDSMSC Algorithm Outline

The most important component of the FMDSM, NMO-SCTT, and FMDSMSC algorithms is source wave ray tracing from source to receiver. Baziw (2002) outlines in detail the governing equations for the seismic ray tracing for the FMDSM and NMO-SCTT cases where there are horizontal and slant planes. In Fig. 8, V_1 to V_{n+1} represent the consecutive vertices of the seismic ray as it travels from the source to the DST receiver. V_1 identifies the source Cartesian coordinates (x_1, y_1, z_1) while V_{n+1} identifies the DST receiver Cartesian coordinates (x_{n+1}, y_{n+1}, z_{n+1}). It is required to trace the ray by determining the Cartesian coordinates of the vertices V_2 to V_n by implementing Fermat's principle and with the following data specified:

- The initial source and receiver Cartesian coordinates.
- The two dimensional Cartesian plane interface equations where the vertices V_2 to V_n lie

$$A_i x + C_i z + D_i = 0, \quad i = 2, \cdots, n \qquad (2)$$

where the parameters A_i, and C_i define the normal to the interface plane and parameter Di is derived by specifying a point on the plane.

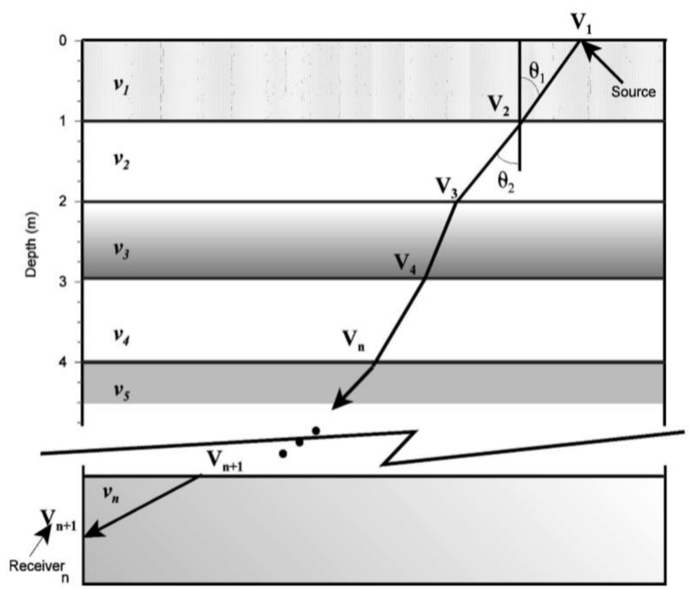

Figure 8: . Refraction of source wavelet as it travels from source to receiver (Baziw, 2002).

- The interval velocities, v_i, $i = 2,\ldots, n+1$. Variable v_i denotes the constant velocity between interfaces $i–1$ and i, (i.e., along the segment of the ray between vertices V_{i-1} and V_i), v_2 is the velocity between the source and V_2, and v_{n+1} is the velocity between the DST receiver and vertex Vn.

Fermat's principle of least time states that a wave will take the ray path for which the travel time is stationary with respect to minor variations of the ray path, that is, the change in travel time for an incremental change in ray path is zero. This principle leads to the condition that the ray path travels along the trajectory that requires minimum time between points. The travel time t along the ray V_1 to V_{n+1} in two dimensions is given by the sum

$$t \;=\; \textstyle\sum_{i=2}^{n+1}[(x_i - x_{i-1})^2 + (z_i - z_{i-1})^2]^{1/2} v_i^{-1} \tag{3}$$

For the FMDSM and NMO-SCTT cases where there are horizontal planes ($A_i = 0$ and $C_i = 1$) and slant planes ($A_i \neq 0$ and $C_i \neq 0$) the travel time t in eq. (3) is expressed in terms of the x coordinate. To adhere to the requirement of Fermat's principle, the partial derivatives of t with respect to x_i are taken and set to zero as follows:

$$\begin{aligned}\frac{\partial t}{\partial x_i} \;=\; & \left[x_i - x_{i-1} \;-\; \frac{A_i}{C_i}(z_i - z_{i-1})\right] / [(x_i - x_{i-1})^2 + (z_i - z_{i-1})^2]^{1/2} v_i \;+ \\ & \left[x_i - x_{i+1} \;-\; \frac{A_i}{C_i}(z_i - z_{i+1})\right] / [(x_i - x_{i+1})^2 + (z_i - z_{i+1})^2]^{1/2} v_{i+1} \\ & = 0, \quad i = 2, .., n\end{aligned} \tag{4}$$

Equation (4) is derived by carrying out the x_i terms in eq. (3) and utilizing eq. (2) to define z_i as a function of x_i (note: $\frac{\partial z_i}{\partial x_i} \;=\; -\frac{A_i}{C_i}$)). The solution to the ray tracing problem is satisfied if the 2n – 2 equations defined by eq. (4) hold simultaneously. The multidimensional Newton-Raphson iteration technique is used to solve eq. (4). The Newton-Raphson technique requires that initial vertices V_2 to Vn be specified that are iteratively updated so that eq. (4) holds. Straight ray paths are assumed between source and receivers when specifying the initial vertices.

In the FMDSMSC stone columns tomographic imaging algorithm there are horizontal ($A_i = 0$ and $C_i = 1$) and vertical intersecting planes ($A_i = 1$ and $C_i = 0$) as opposed to slant planes. For the vertical pane it is required that t be stationary for small variations in the ray path along the vertical plane. Similar to eq. (4) we have

$$\begin{aligned}\frac{\partial t}{\partial z_i} \;=\; & \left[z_i - z_{i-1} \;-\; \frac{C_i}{A_i}(x_i - x_{i-1})\right] / [(x_i - x_{i-1})^2 + (z_i - z_{i-1})^2]^{1/2} v_i \;+ \\ & \left[z_i - z_{i+1} \;-\; \frac{C_i}{A_i}(x_i - x_{i+1})\right] / [(x_i - x_{i+1})^2 + (z_i - z_{i+1})^2]^{1/2} v_{i+1} \\ & = 0, \quad i = 2, .., n\end{aligned} \tag{5}$$

Since where $A_i = 1$ and $C_i = 0$ eq. (5) becomes:

$$\frac{\partial t}{\partial z_i} = \frac{[z_i - z_{i-1}]}{[(x_i - x_{i-1})^2 + (z_i - z_{i-1})^2]^{\frac{1}{2}} v_i} + \frac{[z_i - z_{i+1}]}{[(x_i - x_{i+1})^2 + (z_i - z_{i+1})^2]^{\frac{1}{2}} v_{i+1}} = 0, \quad i = 2, .., n \tag{6}$$

For the horizontal plane $A_i = 0$ and $C_i = 1$ and eq. (4) becomes:

$$\frac{\partial t}{\partial x_i} = \frac{[x_i - x_{i-1}]}{[(x_i - x_{i-1})^2 + (z_i - z_{i-1})^2]^{\frac{1}{2}} v_i} + \frac{[x_i - x_{i+1}]}{[(x_i - x_{i+1})^2 + (z_i - z_{i+1})^2]^{\frac{1}{2}} v_{i+1}} = 0, \quad i = 2, .., n \tag{7}$$

Similar to the FMDSM and NMO-SCTT, the solution to the FMDSMSC ray tracing problem is satisfied if the 2n – 2 equations defined by eqs. (6) and (7) hold simultaneously. Again the multidimensional Newton-Raphson iteration technique is used to solve eqs. (6) and (7) (Baziw, 2002). The FMDSMSC algorithm implements a Monte Carlo technique similar to the NMO-SCTT algorithm where numerous searches are carried out when finding the optimal 2D interval velocities. The Monte Carlo technique is implemented to address the need to search a solution space for the interval velocities with numerous local minima.

3.2 FMDSMSC - Test Bed Example:

Table 1 below provides the working parameters for a test bed simulation of the FMDSMSC. In this test bed simulation the sensor-source offset is 4m (i.e., $\boldsymbol{l_1}$ = 4m in Fig. 6), the stone column diameter is 1m (i.e., $\boldsymbol{l_2}$ = 1m in Fig. 6), and the source-stone column offset is 2m (i.e., $\boldsymbol{l_3}$ = 2m in Fig. 6). The assumed soil interval velocities (V_1 to V_{11} in Fig. 1) are outlined in column 3 of Table 1. A stone column shear wave velocity of 800m/s is assumed. The minimum and maximum values set in the FMDSMSC algorithm for the stone column interval velocities are 650m/s to 1250m/s, respectively. Table 1 shows arrival times derived for the true interval velocities and stone column velocity specified after implementing Fermat's Principle of least time. There several examples where there are faster arrival times for deeper source waves (34.897 at 8m and 37.447) making the application of a straight ray analysis impossible.

Table 1 outlines the estimated FMDSMSC interval velocities (column 4) and associated arrival time residuals (column 5). Column 6 in Table 1 shows the percent difference between the estimated and true interval velocities. As is evident from columns 4 to 6 of Table 1 the estimated interval velocities are very close to the true interval velocities with associated low error residuals and percent differences. The stone column interval velocity was estimated to be 788.9m/s compared to the true values of 800m/s (0.6% difference) . Column 7 of Table 1 outlines the estimated soil interval velocities if a Straight Ray Assumption (SRA) is implemented. As is evident from the nonsensical SRA results, it is mandatory to utilize a tomography algorithm that implements Fermat's principle when estimating in-situ interval velocities when stone columns are present.

Figure 9 illustrates the source wave raypaths as the source waves travel through the stone column to the DST receivers. As is shown in Fig. 9 and according to Fermat's Principle, the seismic waves prefer travelling in the faster velocity stone column and spending a minimal amount of time in the slower interval velocity soil layers. As a result there can be (in this case there are) so-called negative relative arrival times in certain instances.

Table 1. FMSDMSC Test Bed Example Parameters

Depth [m]	Arrival Time [ms]	True Soil Interval Velocity [m/s]	FMDSMSC Estimated Interval Velocities [m/s]	FMDSMSC Residual Error [ms]	Percent Difference [%]	SRA Estimated Interval Velocities [m/s]
2	42.557	100	100.3	0.0049	0.1	126.5
3	33.539	200	201.5	0	0.4	-49.4
4	32.315	260	263.8	0.0001	0.7	-467.5
5	37.846	150	150.9	0	0.3	120.8
6	35.064	250	256.6	0	1.3	-265.7
7	34.878	300	311.1	0	1.8	-4258.5
8	34.897	360	378.4	0	2.5	43771.4
9	37.447	280	289.5	0	1.7	337.9
10	41.767	200	203.5	0	0.9	204.8
11	38.795	350	376.9	0	3.7	-303.7
12	44.897	150	152.0	0	0.7	150.3

***Stone Interval Velocity Estimate = 788.9m/s (0.6% difference).**

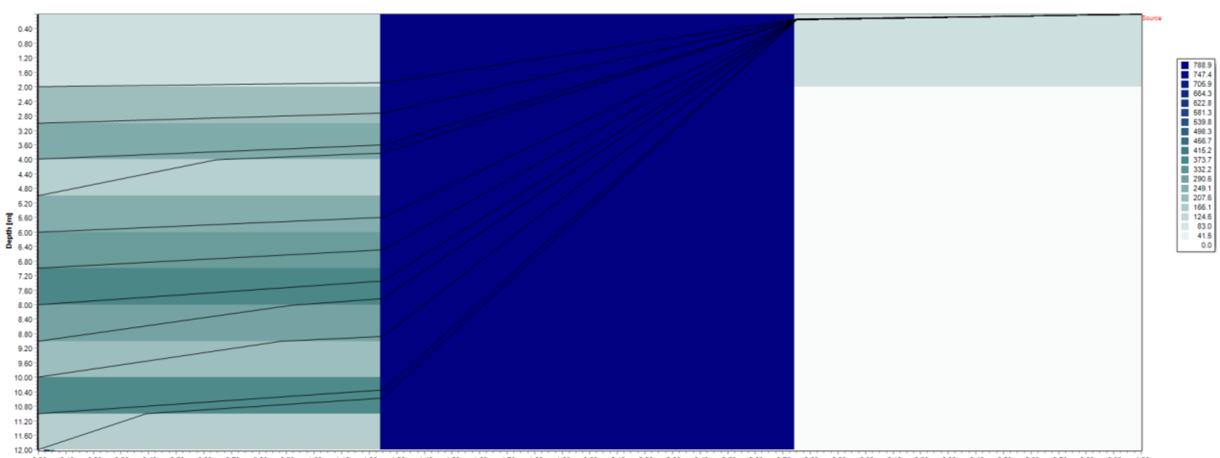

Figure 9. Schematic illustrating the source wave raypaths as the source waves travel through the stone column to the DST receivers and utilizing Fermat's principle.

CONCLUSIONS

This paper has outlined a unique DST testing configuration and tomographic algorithm for characterizing sites which contains stone columns. This new technique is referred to as the Forward Modeling Downhill Simplex Method Stone Columns (FMDSMSC). Stone columns are used in geotechnical site improvement to reduce settlement of foundations, increase load-bearing capacity, improve slope stability and increase the shear strength of a soil. The FMDSMSC was developed by implementing the normal moveout tomographic NMO-SCTT algorithm with significant modifications/additions. The most significant difference between the NMO-SCTT and FMDSMSC algorithms is that the NMO-SCTT models slant and horizontal planes while the FMDSMSC models vertical and horizontal planes. The FMDSMSC algorithm implements a Monte Carlo technique where numerous searches are carried out when finding the optimal 2D interval velocities. The Monte Carlo technique is implemented to address the need to search a solution space for the interval velocities with numerous local minima.

The FMDSMSC technique automatically provides for an error estimate, which is equal to the residual between the synthetic and measured source wave arrival times for each depth increment. The implementation and performance of the FMDSMSC algorithm was demonstrated by considering a challenging test bed example. In a future paper the authors intend to demonstrate the algorithm with actual field data and compare it with a standard SCPT where SRA is applied, which should further demonstrate the validity of this new field procedure and technique.

REFERENCES

Aki, K. and Richards, P.G. (2002), Quantitative Seismology, 2nd edition, Sausalito, California: University Science Books.

ASTM (American Standards and Testing Methods). (2017). “D7400: Standard Test Methods for Downhole Seismic Testing.” ASTM Vol. 4.09 Soil and Rock (II): D5877-latest.

Baziw, E. (2002), "Derivation of seismic cone interval velocities utilizing forward modeling and the downhill simplex method". Can. Geotech. J., 39(5), pp.1181-1192.

Baziw, E., and Verbeek, G. (2012). “Deriving interval velocities from downhole seismic data”. Geotechnical and Geophysical Site Characterization 4 – Mayne (eds), CRC Press, 1019–1024.

Baziw, E. and Verbeek, G (2014a), “Signal Processing Challenges when Processing DST and CST Seismic Data containing TIRs”, ASTM International - Geotechnical Testing Journal (GTJ), vol. 37., no. 3, pp. 1-21.

Baziw, E. and Verbeek, G. (2014b). “Identifying critical layers using SCPT and seismic source moveout”. In Proc. of the 3rd International Symposium on Cone Penetration Testing, CPT'14, May 12-14, 2014 - Las Vegas, Nevada, 357-364.

Baziw, E. and Verbeek, G (2014c), “Methodology for Processing Seismograms Containing Total Internal Reflections”, IEEE Transactions on Geosci. Remote Sensing (TGRS), vol. 52, Issue 11, pp. 7073-7085.

Baziw, E. and Verbeek, G. (2018), "NMO-SCTT: a unique SCPT tomographic imaging algorithm". In Proc. of the 4th International Symposium on Cone Penetration Testing (CPT'18), 21-22 June, 2018, Delft, The Netherlands, 137-142.

Billoet, G. and Gauthey, J.R. (2011), “Recommendations for the design, calculation, construction and quality control of stone columns under buildings and sensitive structures”, USG, the French geotechnical union association Version No. 2 - March 16, 2011, pp. 1-32.

Carvajal, E., Vukotić, G., Castro, J., and Wehr, W. (2013),”Comparison between theoretical procedures and field test results for the evaluation of installation effects of vibro-stone columns”. In Proc. International Conference on Installation Effects in Geotechnical Engineering. Rotterdam. GEO-INSTALL.

Fernando, V, A., Atukorala, U. and Thurairajah, U. (2015), "Ground Improvement Using Vibro Replacement Stone Column Technique and Quality Assurance for New LNG Tank on Tilbury Island, Delta, British Columbia, Canada". In Proc. International Conference on Geotechnical Engineering, August, 2015, Colombo, Sri Lanka, 379-382.

Kirsch, F. (2006), “Vibro stone column installation and its effect on ground improvement”. In Numerical Modelling of Construction Processes in Geotechnical Engineering for Urban Environment; Taylor & Francis: London, UK, 2006; 115–124.

Levent Selcuk, L. and Kayabali, K. (2015), “The design of stone column applications to protect against soil liquefaction”. International Journal of Geotechnical Engineering 9(3): pp. 279-288.

Mccabe, B. and Mcneill, J. (2006), “Vibro-techniques for ground improvement in Ireland”. The Engineers Journal, vol.60, issue.3, pp.181-182.

Ng, K.S., and Tan, S.A. (2015), “Simplified homogenization method in stone column designs”. Soils Found 55(1), pp.154–165.

Sexton, B. G., McCabe, Bryan A., Karstunen, M. and Sivasithamparam, N. (2016). Stone column settlement performance in structured anisotropic clays: the influence of creep. Journal of Rock Mechanics and Geotechnical Engineering 8 (5), 672-688

Sondermann, W., Raju, V.R., Daramalinggam, and Yohannes, M. (2016), “Practical design of vibro stone columns”. In Proc. of the HKIE Geotechnical Division Annual Seminar, Hong Kong, pp. 169-182.